General Disclaimer

One or more of the Following Statements may affect this Document

- This document has been reproduced from the best copy furnished by the organizational source. It is being released in the interest of making available as much information as possible.

- This document may contain data, which exceeds the sheet parameters. It was furnished in this condition by the organizational source and is the best copy available.

- This document may contain tone-on-tone or color graphs, charts and/or pictures, which have been reproduced in black and white.

- This document is paginated as submitted by the original source.

- Portions of this document are not fully legible due to the historical nature of some of the material. However, it is the best reproduction available from the original submission.

Produced by the NASA Center for Aerospace Information (CASI)

NASA Technical Memorandum 79080

(NASA-TM-79080) HIGH TEMPERATURE DYNAMIC MODULUS AND DAMPING OF ALUMINUM AND TITANIUM MATRIX COMPOSITES (NASA) 37 p HC A03/MF A01 CSCL 11D

N79-16077

Unclas
G3/24 43646

HIGH TEMPERATURE DYNAMIC MODULUS AND DAMPING OF ALUMINUM AND TITANIUM MATRIX COMPOSITES

J. A. DiCarlo
Lewis Research Center
Cleveland, Ohio 44135

and

J. E. Maisel
Cleveland State University
Cleveland, Ohio 44115

TECHNICAL PAPER to be presented at the
Symposium on Advanced Fibers and Composites for
Application at Elevated Temperatures
sponsored by The Metallurgical Society of AIME
New Orleans, Louisiana, February 18-22, 1979

HIGH TEMPERATURE DYNAMIC MODULUS AND DAMPING OF ALUMINUM AND TITANIUM MATRIX COMPOSITES

J. A. DiCarlo
National Aeronautics and Space Administration
Lewis Research Center
Cleveland, Ohio 44135

and

J. E. Maisel
Cleveland State University
Cleveland, Ohio 44115

Abstract

Dynamic modulus and damping capacity property data were measured from 20° to over 500° C for unidirectional B/Al (1100), B/Al (6061), B/SiC/Al (6061), Al_2O_3/Al, SiC/Ti-6Al-4V, and SiC/Ti composites. The measurements were made under vacuum by the forced vibration of composite bars at free-free flexural resonance near 2000 Hz and at strain amplitudes below 10^{-6}. Whereas little variation was observed in the dynamic moduli of specimens with approximately the same fiber content (50%), the damping of B/Al composites was found at all temperatures to be significantly greater than the damping of the Al_2O_3/Al and SiC/Ti composites. Because this modulus and damping behavior could be explained very well by composite theory based on constituent phase properties, it follows that phase and composite dynamic properties can now be predicted for test conditions not covered in this study. For those few situations where slight deviations from theory were observed, the dynamic data were examined for information concerning microstructural changes induced by composite fabrication and thermal treatment. Thus, the 270° C damping peak observed in B/Al (6061) composites after heat treatment above 460° C appears to be the result of a change in the 6061 aluminum alloy microstructure induced by interaction with the boron fibers. The growth characteristics of the damping peak suggest its possible value for monitoring fiber strength degration caused by excess thermal treatment during B/Al (6061) fabrication and use.

E-9901

Introduction

As discussed by Lazan (1), studies of the dynamic modulus and damping of structural materials can provide valuable information in the areas of engineering, materials science, and nondestructive evaluation. In the engineering area, dynamic property data are required to understand and predict the intrinsic mechanical response of a material under vibratory and impact loading. In the materials science area, the damping property is an effective scientific tool for monitoring a material's microstructure through the time-dependent deformation mechanisms operating within it. In the nondestructive evaluation (NDE) area, the dynamic characteristics can yield information concerning microstructure responsible for significant quasi-static mechanical properties such as tensile strength. It was, in fact, with the goal of obtaining information in all three areas that a survey study was initiated to measure the dynamic response of selected composite materials. In this paper we report dynamic property data for as-fabricated and heat-treated unidirectional aluminum and titanium matrix composites tested under vacuum from 20^{o} to over 500^{o} C. These baseline data were measured near 2000 Hz in the strain amplitude-independent region below 10^{-6}. The composite systems studied were selected because their structural application is of current aerospace interest, for example, for fan or compressor blades, and because their dynamic behavior would elucidate some significant fundamental differences in the mechanical behavior of the constituent phases. These phases included various alloy matrices and various types of fiber reinforcement such as boron (B), silicon carbide-coated boron (B/SiC), alumina (Al_2O_3), and silicon carbide (SiC) fibers.

Besides the gathering of dynamic property data, another prime objective of this study was to verify that these data were predictable from composite theory and the dynamic properties of the fiber and matrix phases. If composite theory were found applicable, it should then be possible to predict dynamic response for conditions not covered in the test, such as other fiber volume fractions and stress application times (i.e., vibration frequencies). A secondary objective was to search for any differences between data and theory which could be attributed to microstructural or macrostructural changes induced by the fabrication and heat treatment conditions. If these changes could be correlated with a mechanical property such as composite strength, the dynamic data might then be exploited for their NDE value. For the tested aluminum and titanium matrix composites,

it will be shown that the majority of the dynamic data were predictable from composite theory and that wherever slight deviations from theory occurred, important microstructural and NDE information could be extracted.

Experimental

Property Measurement

The apparatus employed for measuring the low strain dynamic modulus and damping of composite materials from -200° to over 500° C is described in detail elsewhere (2). For this paper the basic test method consisted of the forced flexural vibration of a long composite bar at its fundamental free-free resonant mode in a high vacuum furnace ($<10^{-6}$ torr). Because the test objective was to determine properties as a function of temperature, the effects of in-situ high vacuum heat treatment could also be examined. The specimens were cut from thin composite panels into rectangular parellelepipeds with nominal dimensions of 2- by 10- by 100 mm. Specimen support was maintained by four pins located along the specimen length at the two nodes for fundamental resonance which occurred between 1200 and 2200 Hz for the specimens of this study. Vibration drive and detection were achieved electrostatically by two capacitor-type electrodes positioned at convenient antinodes. Because of the low electrostatic forces, vibrational strain amplitudes did not exceed 10^{-6}. During warm-up and cool-down runs at a typical rate of 2° C/min, temperatures measured by a thermocouple at a pin tip were determined to be within ±2° C of the true specimen temperature. For this work, specimen resonance during thermal cycling was automatically maintained by an electronic closed loop. This advantageous self-drive feature was accomplished by inserting a constant output log amplifier and a variable attenuator between the detector lock-in amplifier and the drive audio amplifier.

The flexural dynamic storage Young's modulus E_B (hereafter referred to simply as dynamic modulus) was calculated from the specimen dimensions and the experimental drive frequency $\omega/2\pi$ required for resonance (maximum vibrational displacement). In particular

$$E_B = \frac{12\,\omega^2}{b^2}\left[\frac{m}{w}\left(\frac{\ell}{h}\right)^3\right] \qquad (1)$$

where b is a constant and m, h, w, and ℓ are the specimen mass,

thickness, width, and length, respectively. For $\ell/h > 100$ and fundamental resonance, $b = 22.37$. For $\ell/h < 100$, the b value is smaller but predictable from specimen dimensions (2, 3). Due to the low matrix moduli and finite number of plies N for the composite specimens, E_B was slightly less than the dynamic modulus one would measure, for example, by pure longitudinal waves along the specimen length. However, it can be shown (2) that for typical unidirectional composites, this modulus difference is less than 1 percent when $N \geq 8$. Since this was the case for the composites of this study, it was assumed that the calculated E_B was equivalent to the dynamic axial modulus E_{11} or to the dynamic transverse modulus E_{22} depending, respectively, on whether the fibers were parallel (axial mode) or perpendicular (transverse mode) to the specimen length.

The damping capacity ψ of a material is a measure of intrinsic mechanical energy losses that occur during vibratory motion. These losses are a consequence of microstructural deformation mechanisms whose dynamic stress-strain curves are characteristically hysteretic. Some mechanisms such as dislocation unpinning produce losses which are independent of vibration frequency but increase strongly with vibration strain amplitude; whereas other mechanisms such as dislocation and grain-boundary relaxation produce losses which vary with frequency but are generally amplitude-independent or anelastic (4). In this study the sum total of all hysteretic losses was measured by oscilloscope photographs of the freely decaying detector signal obtained by disconnecting the drive voltage. It was observed that at strain amplitudes below 10^{-6} all decays were exponential with decay time constants independent of initial strain amplitude (linear anelasticity). For this reason, ψ which is defined as $\Delta W/W$, the relative amount of stored energy lost per cycle, was calculated from

$$\psi \equiv \frac{\Delta W}{W} = \frac{4\pi \ln(S_1/S_2)}{\omega(t_2 - t_1)} \qquad (2)$$

where S_1 and S_2 are the detector envelope signals at times t_1 and t_2, respectively. Because the ψ measurement was made in high vacuum, essentially all damping could be attributed to intrinsic losses. Apparatus losses and thermoelastic losses (cf. Appendix) were estimated to contribute less than 0.0003 to the ψ value. Absolute error in the damping measurement was estimated at less than ±5%.

Specimens

Tables 1 and 2 list relevant physical data for the composite specimens and their constituent phases, respectively. A bulk 6061 aluminum alloy specimen was also studied for calibration and control purposes. All composite specimens except Al_2O_3/Al were cut with a diamond wheel from 8 or 16 ply composite panels manufactured by the high temperature diffusion bonding of monolayers. The bonding temperature was $460^{\circ} \pm 5^{\circ}$ C for all TRW boron/aluminum specimens (12) but was unknown for the other specimens. A vacuum infiltration technique was employed for fabrication of the Al_2O_3/Al specimen (6). Fiber volume fractions v_f were determined both by fiber count and by density considerations.

Results and Discussion

Dynamic Modulus

The E_{11} and E_{22} values measured at 22° C for the as-fabricated specimens are listed in Table 3. The absolute error of ~4% arises for the most part from two experimental problems. First, the thicknesses of specimens cut from composite panels were found to be nonuniform, exhibiting variations of as much as 6% along the specimen length. To account for this problem in the moduli calculations two thickness values were used: $\bar{h}$ the average thickness as measured by micrometer and h^* the effective thickness calculated from specimen volume as measured by hydrostatic weighing. Generally, $\bar{h}$ was greater than h^* by less than 1% due perhaps to thickness undulations created by fibers just below the surface. A second problem was that most specimens vibrated at two fundamental resonant modes close in frequency ($\Delta\omega/2\pi \cong 30$ Hz). Although introducing some uncertainty in the modulus data, the two modes differed in amplitude by a factor of 10 or greater (same drive force) so that no beating effects were observed in the damping data. The source of this double mode was unknown but may have been caused by slight inaccuracies in placement of the pin supports at the two vibrational nodes. The moding effect was not limited to the composite specimens as it was observed to be the prime error source for the modulus data of the calibration 6061 aluminum bar.

To determine whether the Table 3 results were predictable from composite theory, calculations of theoretical dynamic moduli were made using the complex modulus approach in the manner described by Hashin (13). For axial vibrations one finds that the rule-of-mixtures (ROM) predicts

$$E_{11} = v_f E_f + v_m E_m \tag{3}$$

where v is volume fraction, E is dynamic modulus, and the subscripts f and m refer to the fiber and matrix phases, respectively. For transverse vibrations, the Halpin-Tsai approximate equation predicts that

$$E_{22} = E_m(H/J) \tag{4}$$

where

$$H = (1 + \zeta v_f)E_f + \zeta(1 - v_f)E_m$$

$$J = (1 - v_f)E_f + (\zeta + v_f)E_m$$

and the ζ parameter is a measure of reinforcement which depends on boundary conditions (14). The predictions of the above equations which were derived under the assumption of low damping and modulus isotropy for each phase are shown in Table 3. These calculations employed the moduli data of Table 2 plus a ζ value of 2. This value was based on the observance that the fiber packing geometry for the transverse specimens was best approximated by a square array (14). The errors in the theoretical moduli of Table 3 are due both to the variation in moduli for the constituent phases (cf. Table 2) and to the experimental errors in the volume fraction determinations (cf. Table 3).

Comparing the experimental and theoretical data of Table 3, one finds good agreement between measured and predicted room temperature moduli. This result confirms both the predictive accuracy of Eqs. (3) and (4) and the experimental accuracy of the modulus measurement technique. This being the case, it would appear then that if experimental errors were reduced, the composite modulus measurement could be employed to accurately determine the average dynamic modulus of a large group of fibers. Along these lines, the Table 3 results suggest in general that the average dynamic modulus for B/SiC is somewhat higher than the Table 2 value, whereas the B, Al_2O_3, and SiC moduli of Table 2 are fairly accurate. However, differences on the low side are also apparent, for example, in the two Avco B/Al (6061) specimens from the same panel and the NASA SiC/Ti specimen. The implication of lower fiber moduli for these composites may be a geometry effect created by internal variation in fiber alignment, a real fiber modulus effect created by differences in fiber fabrication techniques, or an interfacial effect created by poor fiber-matrix bonding within these

specimens. Confirmation of this last effect would give additional value to the dynamic modulus measurement for the detection of flaws in composite macrostructure. For this study, however, experimental modulus errors plus the unknown variation in fiber moduli and alignment preclude any definite conclusions concerning integrity of interfacial bonding within the as-fabricated composites.

Heat treatment and thermal cycling effects were studied by slowly warming to various temperatures, remaining at these temperatures from 10 to 60 minutes, and then furnace cooling down to room temperature. For all but one specimen no frequency shifts outside the double mode range were observed after one to four thermal cycles up to 550° C. The only exception to this constant modulus behavior was the Avco B/Al (6061) axial specimen whose modulus dropped 6% after two cycles to 450° C. Since Table 3 indicates an apparently low modulus for this specimen in the as-fabricated condition, the cycling effect suggests further deterioration of an originally poor interfacial bond.

Regarding temperature dependence of the composite moduli, it was convenient to calculate the dynamic modulus ratio R_x defined as $E_x(T)/E_x(22^\circ\ C)$. The property R_x can be measured quite accurately because it eliminates both the dimensional and double resonance problems inherent in the absolute moduli calculations. From Eq. (1), R_{11} for axial specimens is given as

$$R_{11} = \left[\frac{\omega(T)}{\omega(22^\circ\ C)}\right]^2 \frac{(1 + \alpha_{11}\,\Delta T)^3}{(1 + \alpha_{22}\,\Delta T)^4} \tag{5}$$

where $\Delta T = T - 22^\circ\ C$ and α_{11} and α_{22} are the average coefficients for composite axial and transverse thermal expansion, respectively. Likewise, R_{22} for transverse specimens is

$$R_{22} = \left[\frac{\omega(T)}{\omega(22^\circ\ C)}\right]^2 \frac{1}{(1 + \alpha_{11}\,\Delta T)} \tag{6}$$

Expansion coefficients employed to obtain R_{11} and R_{22} are listed in Table 4. For the B/Al specimens, no significant effects due to matrix alloy or SiC fiber coating could be detected in the R_{11} and R_{22} results. These combined data are shown in Fig. 1 with the R_m measured for the

calibration 6061 aluminum bar and the R_f measured for a typical boron fiber near 2000 Hz. Actual data points are not shown because they were taken less than 10^{o} C apart with an average error in R of less than ±0.003. Figure 2 compares the R_{11} data for the Al_2O_3/Al and two SiC/Ti specimens with literature data for SiC and bulk Ti-6Al-4V.

Examination of the Figs. 1 and 2 data reveals that in contrast to the Al_2O_3 and SiC composites, the B/Al moduli show a nonlinear dependence on temperature. This effect is clearly caused by the nonlinear behavior of the boron fiber and aluminum matrix which both begin to show measurable anelasticity in this temperature range. Such nonlinear behavior is not seen in Fig. 2 because the Al_2O_3 and SiC fibers which dominate axial deformation deform elastically at these temperatures. Another fact to be observed in Figs. 1 and 2 is that the R data are in qualitative agreement with composite theory, that is, $R_m < R_{22} < R_{11} < R_f$. Considering the high accuracy of these data, it was of interest to determine whether quantitative agreement also existed.

For the axial R_{11} results one can employ the rule-of-mixtures Eq. (3) in the form

$$R_{11} = \left(\frac{v_f E_f^o}{E_{11}^o}\right) R_f + \left(\frac{v_m E_m^o}{E_{11}^o}\right) R_m \tag{7}$$

where the superscript o refers to 22^{o} C values. The effects of thermal expansion on volume fraction can be calculated from

$$v_f(T) = v_f^o\left[1 - 2\,\Delta T(\alpha_{22} - \alpha_{11})\right] . \tag{8}$$

When the single phase results for R_f and R_m were inserted into Eq. (7), the calculated R_{11} versus temperature curves for both the B/Al and SiC/Ti specimens were found to be somewhat higher than the experimental curves. This result was interpreted as an indication that the R_m for the bulk specimen did not represent the modulus behavior of the matrix. Under this assumption effective R_m^* curves for the matrices were calculated from Eq. (7) and the R_f and R_{11} data. The resulting curves for the aluminum and titanium alloy matrices are shown by the dashed lines of Figs. 1 and 2, respectively. Although a physical model for $R_m^* < R_m$ has yet to be determined, an independent calculation of the aluminum R_m using

R_{22} and R_f data was found to yield the same result as indicated by the open points of Fig. 1. Therefore, at least for high fiber volume fraction composites, it appears that the R_m^* curves are the appropriate curves for determining matrix moduli dependence on temperature.

Summarizing the practical aspects of the modulus results, one can conclude that the rule-of-mixtures and Halpin-Tsai equations can be employed to predict axial and transverse dynamic moduli, respectively, for the unidirectional aluminum and titanium matrix composites of this study. A low number of thermal cycles to 500° C should have negligible effects on these predictions. Deviations from theory may indicate inadequate fiber-matrix bonding during fabrication. In general the phase moduli R_f and R_m^* data presented here should allow composite moduli determination for any temperature from 20° to 500° C, for any volume fraction in the vicinity of 50%, and for vibration frequencies near 2000 Hz. Because anelastic deformation can be described analytically, the effect of frequency on the boron fiber and aluminum matrix moduli can be easily predicted (2). Because of their elastic behavior below 500° C, frequency effects on the moduli of the SiC, Al_2O_3, and titanium phases need not be considered.

Damping

Before examining the damping data for the various specimens, consider through composite theory the role of the constituent phases in these measurements. Employing the complex modulus approach, one finds that the rule-of-mixtures predicts composite damping for axial vibrations to be

$$\psi_{11} = \gamma_{11}\psi_f + (1 - \gamma_{11})\psi_m \tag{9}$$

where

$$\gamma_{11} = v_f(E_f/E_{11}).$$

For transverse vibrations, the Halpin-Tsai equation predicts

$$\psi_{22} = \gamma_{22}\psi_f + (1 - \gamma_{22})\psi_m \tag{10}$$

where

$$\gamma_{22} = v_f\left[(1 + \zeta)^2 E_f E_m/HJ\right]$$

The γ_{11} and γ_{22} parameters are simply the ratios of fiber stored energy to composite stored energy for axial and transverse modes, respectively. Their calculated values for the specimens of this study are listed in Table 4. It should be clear from this table that damping losses within the fiber microstructure can have a significant effect on composite damping, even for transverse vibrations.

B/Al and B/SiC/Al. - The ψ_{11} damping capacity versus temperature spectra for the TRW B/Al axial specimens are shown in Fig. 3. Two scales have been used to better display the large and rapid change in damping observed in these composites. The data points were measured during first warm-up runs for three specimens in the as-fabricated condition. Very little differences in damping were observed even though the specimens contained two different aluminum alloy matrices. In fact most of the scatter was within the damping measurement error of less than ±5%. No systematic studies were made of heat treatment effects that occurred during the first warm-up runs. However, data taken on first cool-downs from 400° C indicated a small drop in the ψ values. The magnitude of the ψ_{11} drop varied from specimen to specimen, but after heat treatment near 460° C, the ψ_{11} curves for the TRW B/Al (6061) specimens reached the same low level indicated by curve a of Fig. 3. Because the treatment temperatures required to decrease ψ_{11} were in the range of primary recrystallization for aluminum, this effect was probably caused by a reduction in the matrix contribution to axial composite damping. That is, recrystallizing aluminum is known to reduce its damping by decreasing dislocation density and increasing grain size (17) (4).

To better appreciate the quantitative phase contributions to the TRW data of Fig. 3, the damping spectra of a boron fiber and the bulk 6061 aluminum specimen were measured. Typical ψ_f spectra measured in flexure near 2000 Hz are shown in Fig. 4 for 203 μm boron fibers after vacuum heat treatment at 400° C and above (curve $\psi_f(a)$) and after air heat treatment at 400° C (curve $\psi_f(b)$). Data points in this figure and following figures have been omitted for clarity. The strong anelasticity of the boron fiber is clearly evident above 200° C where grain-boundary type "sliding" between small boron structural units is thought to be occurring (5). The decrease in low temperature damping by heating in air is considered to be an impurity atom reduction of low energy "sliding" mechanisms. The ψ_m curve measured on the bulk 6061 aluminum is also shown in Fig. 4 after

correction for a small thermoelastic background (cf. Appendix). Because no changes were observed in ψ_m after heat treatments to 550° C, it was assumed to be representative of the matrix material contributing to the curve a of Fig. 3. A ψ_f^* curve representative of the boron fibers within the axial specimens was then calculated using composite theory, that is, Eq. (9). As indicated in Fig. 4 the resulting ψ_f^* curve was found to be in very good agreement with the air-treated ψ_f(b) curve. This result suggests that fiber damping was essentially unaltered by composite fabrication except at low temperature where possible surface contamination effects are evident. From an engineering point of view, it follows from Eq. (9) that the ψ_{11} for a 50 fiber volume percent B/Al composite vibrating near 2000 Hz can range from as low as 0.84 ψ_f^* to as high as the as-fabricated data of Fig. 3, or even higher, depending on the low temperature mechanical history of the matrix. One should expect also that vibrating at strain levels greater than 10^{-6} will produce increases in both fiber (5) and matrix damping. Vibrating at frequencies lower or higher than 2000 Hz will shift damping to lower or higher temperatures, respectively. The magnitudes of these shifts for the boron fiber and aluminum matrix have been discussed elsewhere (2).

The damping results for the Avco B/Al (6061) axial and transverse specimens are shown in Figs. 5 and 6, respectively. Because their ψ_{11} spectra were in excellent agreement, only two curves were required in Fig. 5 to describe the damping data for the Avco B/Al (6061) and B/SiC/Al (6061) axial specimens in the as-fabricated (curve a) and heat-treated near 400° C (curve b) conditions. The effects of heating the B/SiC/Al (6061) specimen to 550° C are shown by the dashed line. Comparing these results with the TRW axial data of Fig. 3, one finds qualitatively similar temperature-dependent behavior. Slight quantitative differences can be seen, however, at 150° C where the as-fabricated Avco ψ_{11} appears to be annealing to lower values, at high temperature where Avco ψ_{11} is less than TRW ψ_{11}, and at 270° C where both the as-fabricated and heat-treated Avco ψ_{11} contain a small damping peak that is absent in the TRW ψ_{11}. At first glance one might attribute these deviations to slightly different matrix microstructures and thus of little consequence. Although this is probably the case for the first two effects, the existence of the damping peak as will be discussed in a later section may have significant practical value.

Regarding the Avco transverse specimens, it should be pointed out that during the initial warm-ups these specimens were found to bend slightly out of plane due probably to variations in the thermal expansion coefficient α_{22}. Because of the small gaps between the electrodes and specimen, this bending effect eventually produced electrical contact, thereby inhibiting further data taking. For this reason, as shown in Fig. 6, the as-fabricated data had to be terminated at 260° C for the B/Al (6061) specimen (curve a) and at 200° C for the B/Al (1100) specimen. Upon termination of the warm-up run, cool-down data was taken, yielding curves b and d for the B/Al (6061) and B/Al (1100), respectively. To achieve higher temperature heat treatments, the gap separations were increased considerably, thus preventing both electrical contact and data taking during the treatment run. After treatment, gap separations were reduced to values suitable for dynamic measurements during the next warm-up. The effect of 1-hour 550° C treatment on the Avco B/Al (6061) is shown by curve c of Fig. 6. This curve which clearly reveals the 270° C damping peak suggests that the heat treatment had little effect on the height of the as-fabricated peak but increased its width on the low temperature side.

To determine whether composite theory would predict the transverse damping capacity results of Fig. 6, the ψ_m and effective ψ_f^* curves of Fig. 4 were inserted into Eq. (10) assuming a 50 fiber volume percent B/Al composite. As shown by the dashed curve of Fig. 6 the calculated ψ_{22} was measurably lower than the experimental background data. This result suggests that the transverse data contained some additional background damping that increased monotonically with temperature. Although the exact source of this damping is presently unknown, some possible explanations include stronger fiber anelasticity for vibrations transverse to the fiber length and/or unexpected thermoelastic energy losses for the transverse specimens (cf. Appendix). Clearly more transverse work must be done using, for example, composites with varying fractions of elastic fibers.

Al_2O_3/Al and SiC/Ti. - The ψ_{11} damping spectra for the Al_2O_3/Al axial specimen are shown in Fig. 7. Curve a is the first warm-up as-fabricated data and curve b the first cool-down data after 10 minutes at 560° C. Comparing these results with the Figs. 3 and 5 data, one observes that at all temperatures the Al_2O_3/Al specimen has significantly less damping than the B/Al axial specimens. This difference can be understood in terms of composite theory and the fact that in contrast to the highly a

anelastic boron fiber, the elastic Al_2O_3 fiber has essentially no damping. For example, assuming $\psi_f = 0$ for the Al_2O_3 fiber, Eq. (9) predicts that $\psi_{11} = 0.16\ \psi_m$ so that the Fig. 7 data represents matrix behavior reduced by a factor of 6. Although exact verification of this numerical relationship is difficult because metal matrix damping is highly structure sensitive, approximate agreement can be found by comparing the Fig. 7 data with the 6061 aluminum data of Fig. 4. In addition, the primary recrystallization effects observed above 400° C for the Al_2O_3/Al specimen are qualitatively similar to those observed for the B/Al specimens. However, in contrast to the behavior of the 1100 and 6061 aluminum matrices, the Al_2O_3/Al matrix displayed near 375° C a damping peak whose height was apparently unaffected by the 560° C heat treatment. A possible microstructural explanation for its source is the Zener relaxation (4) of substitutional lithium atoms employed in this matrix to improve fiber wetting (6).

The ψ_{11} spectra for the SiC/Ti axial specimens are shown in Fig. 8. For the SiC/Ti-6Al-4V composite, curve a is the first warm-up as-fabricated data and curve b the first cool-down data after 10 minutes at 590° C. Curve c is the first warm-up as-fabricated data for the 25 fiber volume percent SiC/Ti specimen. No cool-down data were taken for this specimen. Comparing these results with the B/Al axial data of Figs. 3 and 5, one observes significantly lower damping at all temperatures for the SiC/Ti specimens, a fact again attributable to the elasticity of the reinforcing fiber. Thus, as was the case for Al_2O_3/Al, the Fig. 8 spectra represent reduced damping behavior of the titanium matrices. Although two different alloys were employed, similar ψ_{11} behavior can be seen especially near 200° and 400° C where annealing effects are apparent and above 500° C where grain boundary relaxation effects begin to predominate (18).

Summarizing the engineering aspects of the composite damping results, one can conclude that the damping of aluminum and titanium matrix composites can be greater than the bulk matrix material if the reinforcement fibers are highly anelastic such as boron, but can be significantly less if the fibers are elastic such as Al_2O_3 and SiC. The magnitude of these effects are predictable by Eqs. (9) and (10) for axial and transverse conditions, respectively. In these relations, it can be assumed that ψ_f for boron is the ψ_f^* of Fig. 4 (corrected, if necessary, for frequency (2)), that $\psi_f = 0$ for Al_2O_3 and SiC, and that ψ_m is the damping of the bulk matrix material. It should also be realized that whereas the damping of the fiber phases ψ_f

are relatively unaffected by mechanical and thermal treatment, minor variations in deformation, heat treatment, or alloy content can cause large variations in matrix damping ψ_m. Thus, on a relative basis, composites reinforced by the elastic fibers could show much larger fluctuations with treatment conditions than composites reinforced by the boron fiber.

Heat Treatment Effects in B/Al (6061)

In our previous study (2), it was observed that as-fabricated B/Al (6061) specimens which displayed the 270° C damping peak had lower tensile strengths than B/Al (6061) specimens without the peak. However, the peak could be created in the stronger specimens by heat treatment at 550° C, a temperature known to degrade fiber strength by reaction between the boron and the aluminum matrix (19). Thus, there exists the possibility that the appearance of the 270° C damping peak is indicative of fiber weakening caused by thermal overprocessing of the composite. To determine whether this is the case, we conducted a study of the effects of heat treatment temperature on the size and shape of the B/Al (6061) damping peak. Our approach was to compare these results with fracture strain data for heat-treated B/Al (6061) axial composites (19). If an empirical correlation could be found between the damping and axial fracture strain data, it should then be possible to employ composite damping to nondestructively evaluate the strength of boron fibers in as-fabricated and heat-treated B/Al (6061) composites.

Because the TRW B/Al (6061) data showed no peak for the as-fabricated condition (30 min at 460° C), the growth characteristics of the damping peak were determined by subjecting an as-fabricated TRW B/Al (6061) axial specimen to 1-hour heat treatments at various temperatures above 460° C. The ψ_{11} damping results presented in Fig. 9 are best fit curves from data points taken less than 5° C apart. To better appreciate the thermally-induced changes in peak shape, the damping background from curve a of Fig. 3 was subtracted from the Fig. 9 data to yield the damping results of Fig. 10. The inverse absolute temperature scale was used here because damping peaks produced by thermally-activated mechanisms are generally symmetric when plotted versus inverse temperature (4). Although measurement and subtraction errors introduced a $\Delta\psi_{11}$ uncertainty of as much as 0.1%, certain growth and shape trends can be ascertained from the Fig. 10 data. For example, after the lowest treatment temperature of 460° C,

a small and apparently symmetrical peak centered near 294° C became evident. After the 480° C treatment, this peak about doubled but retained its shape. Although some increase in peak height was observed after the 500° C treatment, the major damping change was on the low temperature side of the peak, suggesting perhaps the growth of other peaks. Higher temperature treatments had negligible effect on the magnitude of the damping maximum but slightly decreased its temperature location by monotonically increasing the low temperature asymmetry. The Avco B/Al (6061) transverse specimen heat-treated to 550° C also showed evidence of this low temperature damping growth (cf., Fig. 6).

In order to determine whether any correlation could be established between the peak growth characteristics and fiber strength degradation, the B/Al (6061) fracture strain data of Metcalfe and Klein (19) were analyzed in terms of 1-hour heat treatment effects. The results shown by the hatched area in Fig. 11 were cut off at an upper limit of 0.85%, the average fracture strain estimated from strength data for the TRW B/Al (6061) specimens. Comparing these data with the Fig. 10 results, one finds that fiber (or axial composite) fracture strain begins to decrease at approximately the same heat treatment temperature at which composite damping between 200° and 350° C begins to increase. From a materials science point of view, this suggests that the mechanisms for both effects were controlled by the same process, such as boron atom diffusion across the fiber-matrix interface. From an NDE point of view, this suggests that an empirical correlation does exist between peak damping and boron fiber fracture strain. To examine this possibility, we have arbitrarily chosen to plot in Fig. 11 the damping growth at 200° and 250° C. Comparing the Fig. 11 fracture strain and damping results, one finds that since they both depend linearly on temperature, they can indeed be correlated with each other. Thus, any extra composite damping measured over background between 200° and 250° C can be used not only to estimate 1-hour heat treatment temperature but also degradation in boron fiber fracture properties. Of course, the damping data of Fig. 11 apply only to 50 fiber volume percent B/Al (6061) axial specimens vibrating near 2000 Hz. If other volume fractions, fiber layups, or frequencies are used, new calibration curves for heat treatment effects on composite damping would have to be determined.

Regarding a microstructural model for the 270° C damping peak, it appears that the boron fiber and the 6061 aluminum matrix are both required

for the peak's appearance. This follows from the observation that neither the bulk 6061 aluminum specimen nor a TRW B/Al (1100) specimen showed evidence of the peak before or after heat treatment at 550° C. It also appears that the microstructure responsible for the peak is contained within the 6061 matrix and not within the fiber or fiber-matrix interface. As previously discussed (2), this conclusion is based on the fact that the peak was about five times larger in transverse specimens than in axial specimens taken from the same panel (cf., Figs. 5 and 6). From these results one is led toward a model in which during the thermally-induced reaction between the boron fiber and aluminum matrix, boron atoms diffused away from the interface possibly as interstitial atoms to become trapped eventually at substitutional atoms or precipitated phases specific to the 6061 aluminum alloy. The trapping mechanism is required to explain the absence of the peak in the single phase 1100 aluminum matrix and also the very low solubility of boron in aluminum (20). The damping could arise from a stress-induced ordering of boron atoms (4), that is, by an interaction between the applied stress and the boron atoms as they thermally vibrate at their trap sites. Damping maxima would occur then at those temperatures where the boron vibration or jump rate ω_j becomes equal to the angular frequency ω of the applied stress. For thermally activated processes,

$$\omega_j = \omega_o \exp(-Q/kT) \tag{11}$$

where Q is the energy barrier crossed during jumping, k is Boltzmann's constant, and T is the absolute temperature. Typically for point defects, $\omega_o \cong 10^{15}$ so that for the applied stress frequency of 2000 Hz, $Q \cong 1.2$ eV for the initial damping peak centered near $T = 567$ K. The change in peak shape with increasing heat treatment might then be explained by the fact that as new boron atoms enter the matrix, they cluster or interact with each other in such a manner as to reduce the thermal energy barrier Q for the newly arrived atoms, thereby producing new damping maxima on the low temperature side of the initial peak. Similar behavior has been observed in other alloy systems such as manganese steel where the interstitial carbon atoms interact with substitutional manganese atoms to produce a damping peak which grows asymmetrically with carbon content (4).

Finally, the experimental or theoretical situation regarding boron fibers with surface coatings is not clear at the present time. For example, the Avco B/SiC/Al (6061) axial specimen did possess the 270° C damping

peak in the as-fabricated condition, suggesting some boron diffusion through the SiC layer at this specimen's fabrication temperature (unknown). But, in contrast to the Avco B/Al (6061) specimens, the peak did not change after heat treatment at 550^{o} C.

Summary

The principal engineering, scientific, and NDE findings of this study can be summarized as follows:

1. Dynamic modulus and damping capacity property data were measured from 20^{o} to over 500^{o} C for unidirectional B/Al (1100), B/Al (6061), B/SiC/Al (6061), Al_2O_3/Al, SiC/Ti-6Al-4V, and SiC/Ti composites. The measurements were made under vacuum by the forced vibration of composite bars at free-free flexural resonance near 2000 Hz and at strain amplitudes below 10^{-6}.

2. The room temperature dynamic moduli E_{11} and E_{22} were generally in good agreemwnt with the predictions of the rule-of-mixtures and Halpin-Tsai equations for longitudinal stress waves parallel (axial) and perpendicular (transverse) to the fibers, respectively. This result supports (a) the use of these equations for predicting unidirectional dynamic properties at fiber volume fractions and vibrational frequencies not covered in the test results, and (b) the use of the flexural vibration test for monitoring the effects of fabrication and use conditions on phase microstructure and composite macrostructure. Thus, for example, the observance of moduli values lower than those expected theoretically may be an indication for some as-fabricated specimens of less than optimum interfacial bonding.

3. For the temperature dependence of the moduli, the normalized modulus ratio $R_x = E(T)/E(22^{o}\ C)$ was found to be an accurate and reproducible parameter. Comparison of the experimental R_{11} and R_{22} data with the predictions of composite theory based on R data for the constituent phases suggest that the matrix moduli decrease faster with temperature than the moduli of bulk specimens of these metals. For this reason the experimental composite data were employed to construct effective R_m^* curves to be used with the composite equations to describe modulus behavior for both the aluminum and titanium matrices. A low number (<5) of thermal cycles from 20^{o} to near 500^{o} C was generally found to have negligible effects on the R curves and the 22^{o} C moduli.

4. The axial damping capacities ψ_{11} of the B/Al (1100), B/Al (6061), and B/SiC/Al (6061) specimens were observed to be as great and greater than the damping capacity of a bulk 6061 aluminum alloy specimen and significantly greater than the axial damping capacities of the Al_2O_3/Al and SiC/Ti specimens. These results can be explained by the rule-of-mixtures, measured damping for the boron fiber, and the assumption of zero damping for the Al_2O_3 and SiC fibers. Thus the damping of aluminum and titanium matrices are enhanced by boron fiber reinforcement and significantly diluted by Al_2O_3 and SiC fiber reinforcement.

5. Heat treatments to 400^{o} C and above generally produced a slight decrease in the damping-temperature spectra of as-fabricated specimens. This behavior is in most part explainable by annealing or recrystallization effects within the matrix microstructure, leading to a diminution in matrix damping. However, heat treatment of B/Al (6061) specimens above 460^{o} C also produced a damping increase in the form of a peak centered near 270^{o} C. It was determined that growth data for the damping peak could be empirically correlated with literature data for the degradation in fiber fracture strain caused by the thermal-overprocessing of B/Al (6061) composites. On the basic level, this finding implies that the microstructural sources for both effects are controlled by the same process, such as, boron atom diffusion across the fiber-matrix interface. Characteristics of the damping peak suggest that its source is the stress-induced ordering of boron atoms trapped at substitutional atoms or precipitated phases within the 6061 aluminum alloy. On the practical level, the finding of a damping-strength correlation supports the use of composite damping measurements for the nondestructive evaluation of boron fiber strength in as-fabricated and heat-treated B/Al (6061) composites.

Appendix

Thermoelastic Damping

During the flexural vibration of a material, internal transverse temperature gradients are generated due to coupling between local stress and temperature. If the vibrational period of the stress is near the relaxation time for thermal diffusion across the specimen thickness, mechanical energy losses arise producing the thermoelastic damping effect (4). For a thin rectangular cross-section specimen, the resulting damping capacity is predictable from

$$\psi \cong \psi_{max}\left[2\omega\omega_o \Big/ \left(\omega^2 + \omega_o^2\right)\right]$$

where ω is the angular frequency of the applied stress,

$$\omega_o = (K/\rho C)(\pi/h)^2$$

and

$$\psi_{max} = \pi E \alpha^2 T/\rho C$$

Here K, ρ, C, h, E, α, and T are the thermal conductivity, density, specific heat, thickness, Young's modulus, thermal expansion coefficient, and average absolute temperature of the specimen. Because of its high expansion coefficient and low density, aluminum can have a large thermoelastic damping effect, for example, $\psi_{max} = 1.6\%$ at $T = 295$ K. However, for the bulk 6061 aluminum alloy specimen of this study, $\omega_o << \omega$ so that this effect is greatly reduced. In fact, at 295 K a thermoelastic ψ value of 0.024% is predicted and a ψ value of 0.032% was measured, suggesting very small damping contributions from the apparatus and this specimen's microstructure.

For the thermoelastic effect in composites it was assumed that the material properties in the above equations could be replaced by effective composite properties based on the volume fractions and corresponding properties of the constituent phases. Thus for axial vibrations, $E = E_{11}$, $\alpha = \alpha_{11}$, $K = K_{22}$; whereas for transverse vibrations, $E = E_{22}$, $\alpha = \alpha_{22}$, and $K = K_{22}$. Employing composite theory for these thermomechanical properties (21), one finds for the B/Al specimens of this study that

$\psi_{(axial)} = 0.003\%$ and $\psi_{(transverse)} = 0.02\%$. Therefore, although the thermoelastic damping effect for B/Al transverse specimens is a factor of 7 larger than the effect for B/Al axial specimens, it is still quite small for the flexural frequencies of this work.

REFERENCES

1. B. J. Lazan: Damping of Materials and Members in Structural Mechanics, Pergamon Press, Oxford, 1968.
2. J. A. DiCarlo and J. E. Maisel: Presented at the Fifth Conference on Composite Materials: Testing and Design, Am. Soc. for Test. Mater., New Orleans, La., 1978.
3. T. C. Huang: J. Appl. Mech., 1961, vol. 28, pp. 579-584.
4. A. S. Nowick and B. S. Berry: Anelastic Relaxation in Crystalline Solids, Academic Press, New York, 1972.
5. J. A. DiCarlo: in ICCM/2, Second International Conference on Composite Materials, B. Noton, R. Signorelli, K. Street, and L. Phillips, eds., p. 520, The Metallurgical Society of AIME, New York, 1978.
6. A. R. Champion, W. H. Krueger, H. S. Hartmann, and A. K. Dhingra: in ICCM/2, Second International Conference on Composite Materials, B. Noton, R. Signorelli, K. Street and L. Phillips, eds., p. 883, The Metallurgical Society of AIME, New York, 1978.
7. R. H. Ericksen: Fibre Sci. Technol., 1974, vol. 7, pp. 173-183.
8. P. T. B. Shaffer, ed.: Handbook of High-Temperature Materials: No. 1 - Materials Index, Plenum Press, New York, 1964.
9. R. L. Crane: AFML-TR-72-180, 1972, Air Force Materials Laboratory, Wright-Patterson AFB, Ohio, 1972.
10. W. S. Coblenz: J. Am. Ceram. Soc., 1975, vol. 58, pp. 530-531.
11. T. Lyman, ed.: Metals Handbook. Vol. 1, Properties and Selection of Metals, American Society for Metals, Metals Park, Ohio, 1961.
12. P. Melnyk: Private communication.
13. Z. Hashin: Int. J. Solids Struct., 1970, vol. 6, pp. 797-807.

14. J. E. Ashton, J. C. Halpin, and P. H. Petit: Primer on Composite Materials: Analysis, p. 72, Technomic Publ. Co., Stamford, Conn., 1969.

15. K. G. Kreider and V. M. Patarini: Metallurgical Transactions, 1970, vol. 1, pp. 3431-3435.

16. C. J. Smithells, ed.: Butterworths, London, 1976.

17. E. Bonetti, E. Evangelista, P. Gondi, and R. Tognato: Phys. Stat. Sol. (a), 1977, vol. 39, pp. 661-667.

18. S. Mishra and M. K. Asundi: in Titanium Science and Technology, Vol. 2, p. 883, Plenum Press, New York, 1973.

19. A. G. Metcalfe and M. J. Klein: Interfaces in Metal Matrix Composites. Vol. 1, Composite Materials, A. G. Metcalfe, ed., p. 125, Academic Press, New York, 1974.

20. M. Hansen: Constitution of Binary Alloys, p. 70, McGraw-Hill, New York, 1958.

21. B. W. Rosen: Proc. Roy. Soc. Lond. A, 1970, vol. 319, pp. 79-94.

Table 1. - Description of Specimens

Specimen (fiber/matrix)	Manufacturer	Fiber		Number of plies	Density g/cm^3	Test conditions	
		V_f, %	Diameter, μm			Mode[a]	Frequency, Hz
B/Al (1100)	TRW	50	203	8	2.554	AX	2070
	Avco	49	203	8	2.554	TR	1500
B/Al (6061)	TRW[b]	51	203	8	2.552	AX	2000
	Avco	48	203	8	2.560	AX	1870
	Avco	48	203	8	2.560	TR	1360
B/SiC/Al (6061)[c]	Avco	51	145	8	2.598	AX	1650
Al_2O_3/Al[d]	Dupont	52	20	--	3.246	AX	2180
SiC/Ti-6Al-4V	TRW	44	142	16	3.720	AX	2150
SiC/Ti	NASA[e]	25	101	16	4.250	AX	1260
Al (6061)					2.707		1600

[a]AX (axial) and TR (transverse) for fibers parallel and perpendicular to specimen length, respectively.

[b]Includes three different specimens.

[c]Fibers are ~142 μm boron (on tungsten) with ~1.3 μm SiC protective coating.

[d]Matrix is a binary alloy of aluminum and 2% (by weight) lithium (6).

[e]Fabricated and supplied by R. Jech.

Table 2. - Phase Properties at 22° C

Fibers	Diameter, μm	Modulus, GN/m^2	Density, g/cm^3	Thermal expansion coefficient,[a] $^{o}C^{-1} \times 10^6$	Poisson's ratio
B (on W)[b]	203	[c]416±16	2.41	5.0	0.13
B/SiC (on W)[d]	145	[e]422±10	2.50	5.0	.13
Al_2O_3[f]	20	362±17	3.90	[g]6.8	[g].25
SiC (on C)[h]	142	[i]415±10	3.07	[g]4.6	[j].17
SiC (on W)[h]	101	[i]415±10	3.41	[g]4.6	[j].17
Matrices[k]					
Al (1100 or 6061)		69±2	2.70	26	0.33
Al (2% Li)		69±2	2.55	26	.33
Ti (unalloyed)		112±8	4.52	9.4	.36
Ti-6Al-4V		112±8	4.43	10.3	.36

[a]Average value between 20° and 300° C.

[b]Manufactured by Avco. Properties from Ref. 5.

[c]Elastic Young's modulus corrected for anelastic effects near 2000 Hz.

[d]Manufactured by Hamilton Standard. Properties calculated from 142 μm boron fiber with 1.3 μm SiC coating.

[e]From Ref. 7 after correction for 22° C anelastic creep effects (+4%).

[f]Manufactured by Dupont. Properties from Ref. 6.

[g]Ref. 8.

[h]Manufactured by Avco. Properties from Avco data sheet SC-600-874-5M.

[i]Ref. 9.

[j]Ref. 10.

[k]Ref. 11.

Table 3. - Dynamic Moduli at 22° C and ~2000 Hz

Specimen	Fiber volume fraction, v_f, %	Dynamic moduli, GN/m^2		
		Experimental		Theoretical[a]
		E_{11}	E_{22}	
B/Al (1100)	50 ±1	251 ±9	-----	243 ±13
	49 ±1	-----	148 ±8	161 ±8
B/Al (6061)	51 ±1	254 ±6	-----	247 ±13
	48 ±1	220 ±6	-----	236 ±12
	48 ±1	-----	141 ±6	158 ±8
B/SiC/Al (6061)	51 ±1	271 ±13	-----	250 ±10
Al_2O_3/Al	52 ±2	228 ±7	-----	222 ±16
SiC/Ti-6Al-4V	44 ±1	253 ±9	-----	245 ±12
SiC/Ti	25 ±3	171 ±10	-----	188 ±18
Al (6061)	----	71 ±5	-----	69 ±2

[a]From rule-of-mixtures and Halpin-Tsai equations using phase properties of Table 2.

Table 4. - Specimen Expansion and Fiber Fraction Parameters

Specimen type	Fiber volume fraction, v_f	Thermal expansion coefficient,[a] $^{o}C^{-1} \times 10^{6}$		Energy-weighted fiber volume fraction	
		α_{11}	α_{22}	γ_{11}	γ_{22}
B/Al	0.50	5.5	19	0.84	0.31
Al_2O_3/Al	0.52	[b]7.2	[b]18	0.84	----
SiC/Ti	0.44	7.8	8.1	0.75	----
	.25	8.2	8.4	.55	----

[a]When not available in literature, α values were calculated from data and phase theory in Ref. 15.

[b]Ref. 6.

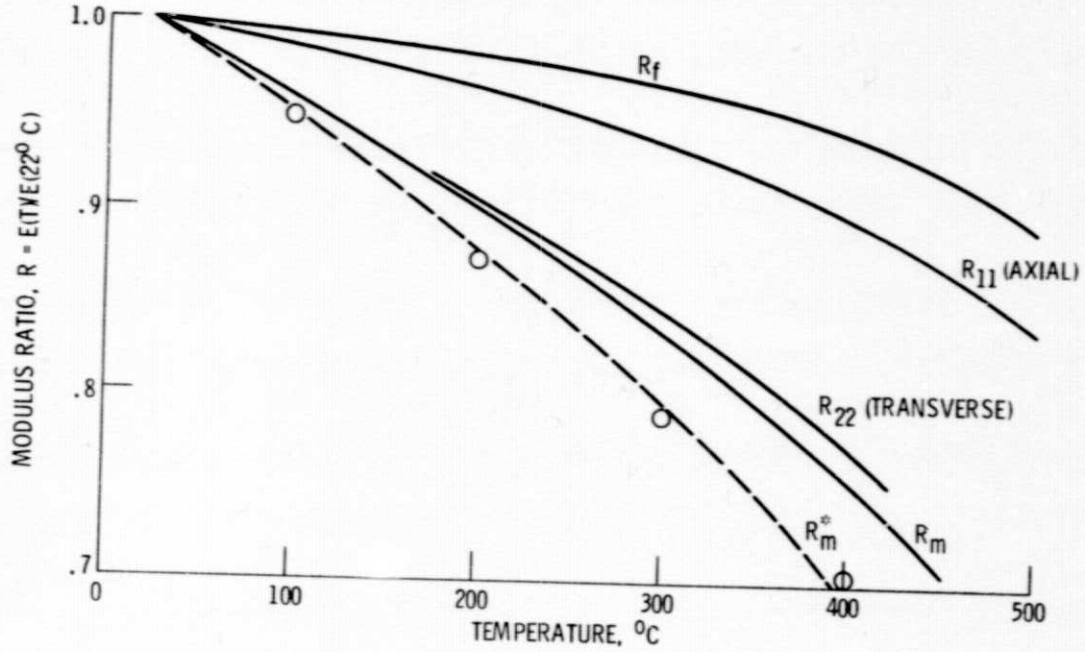

Figure 1. - Temperature dependence of dynamic modulus ratio for the B/Al axial and transverse specimens and their constituent phases. Measurements were made near 2000 Hz at strains $< 10^{-6}$. The R_m^* dashed curve and data points were calculated for the aluminum matrix using the R_{11} and R_{22} data, respectively.

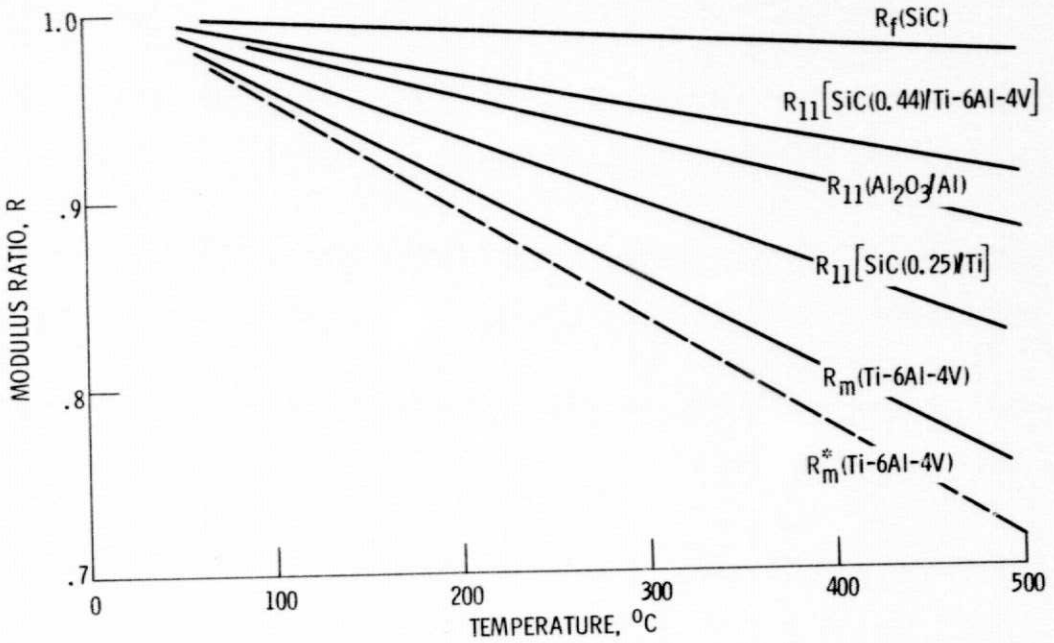

Figure 2. - Temperature dependence of dynamic modulus ratio for the Al_2O_3/Al and two SiC/Ti axial specimens. Measurements were made near 2000 Hz at strains $< 10^{-6}$. The single phase SiC and Ti-6Al-4V data were obtained from references 10 and 16, respectively. The dashed curve is R_m^* calculated for the titanium alloy matrix.

ORIGINAL PAGE IS
OF POOR QUALITY

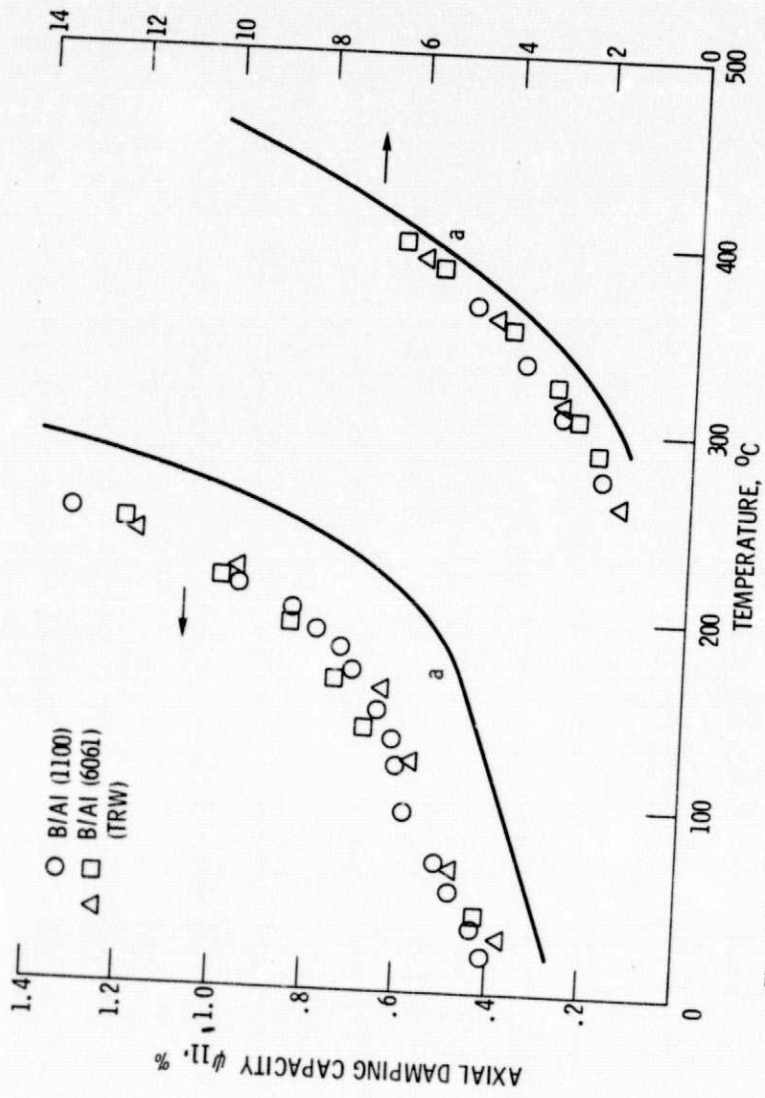

Figure 3. - Temperature dependence of damping for the TRW B/Al (1100) and B/Al (6061) axial specimens in the as-fabricated condition (data points, and for TRW B/Al (6061)) specimens in the heat-treated to 460° C condition (curve a). Damping was measured near 2000 Hz at strains $< 10^{-6}$.

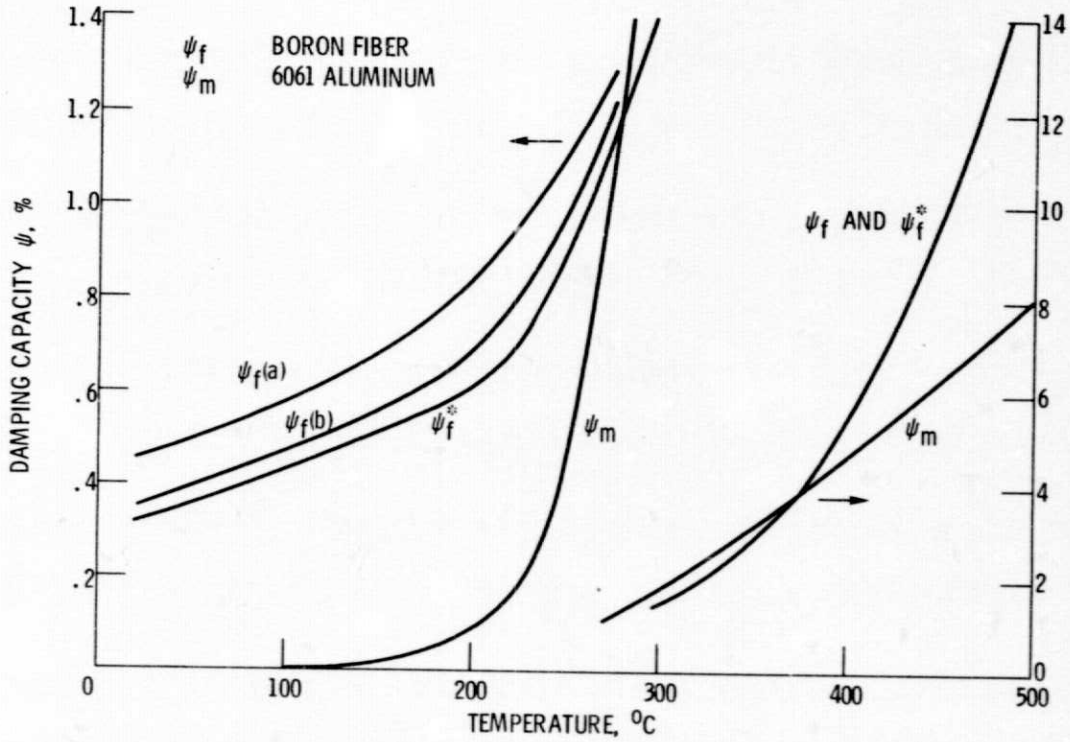

Figure 4. - Temperature dependence of damping for a typical boron fiber (ψ_f) and the bulk 6061 aluminum alloy specimen (ψ_m). Curves $\psi_f(a)$ and $\psi_f(b)$ were measured after 400^0 C vacuum and air treatment, respectively; curve ψ_f^* was calculated for the fiber from the ψ_m curve and ψ_{11} data for heat-treated B/Al (6061). Curve ψ_m was measured for both the as-received and 550^0 C heat-treatment conditions. Measurements were made near 2000 Hz at strains $< 10^{-6}$.

ORIGINAL PAGE IS
OF POOR QUALITY

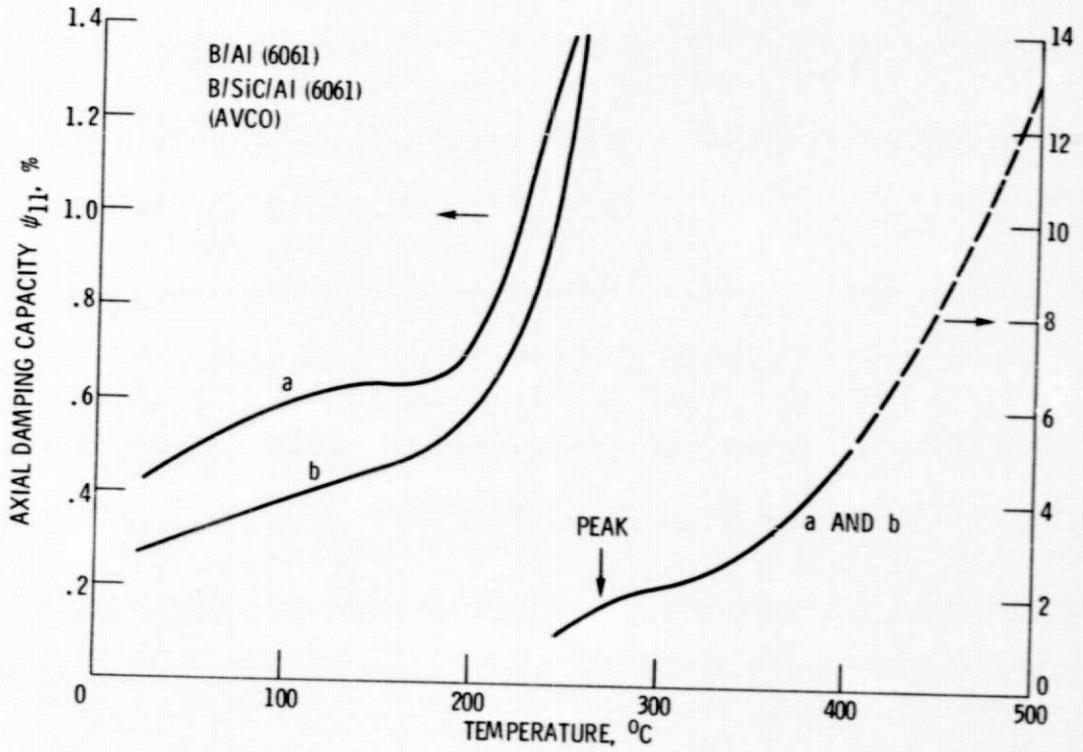

Figure 5. - Temperature dependence of damping for the Avco B/Al (6061) and B/SiC/Al (6061) axial specimens in the as-fabricated (curve a) and the heat-treated at 400° C (curve b) conditions. The dashed curve and curve b are damping for the B/SiC/Al (6061) specimen after heat treatment at 550° C. Measurements were made near 2000 Hz at strains $< 10^{-6}$.

ORIGINAL PAGE IS
OF POOR QUALITY

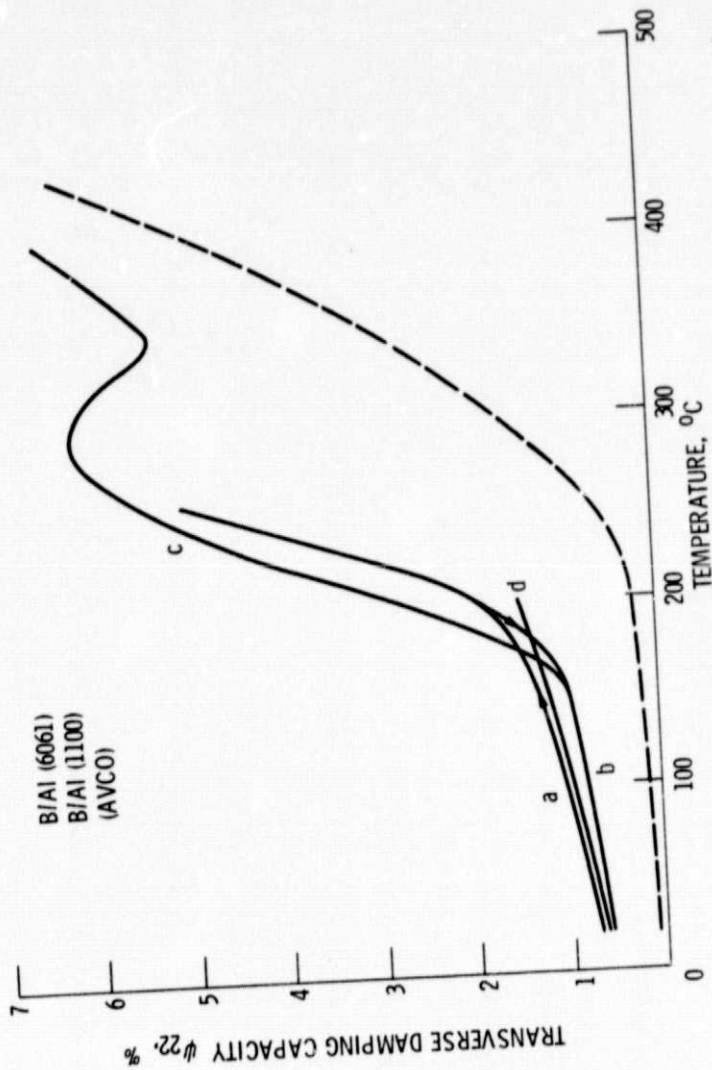

Figure 6. - Temperature dependence of damping for the Avco B/Al (6061) transverse specimen in the as-fabricated condition (curve a) and after heat treatments at 260° C (curve b) and at 550° C (curve c). Curve d is damping for the Avco B/Al (1100) specimen after heat treatment at 200° C. Measurements were made near 1500 Hz at strains $< 10^{-6}$. Dashed curve was calculated from the damping of a boron fiber and the bulk 6061 aluminum specimen.

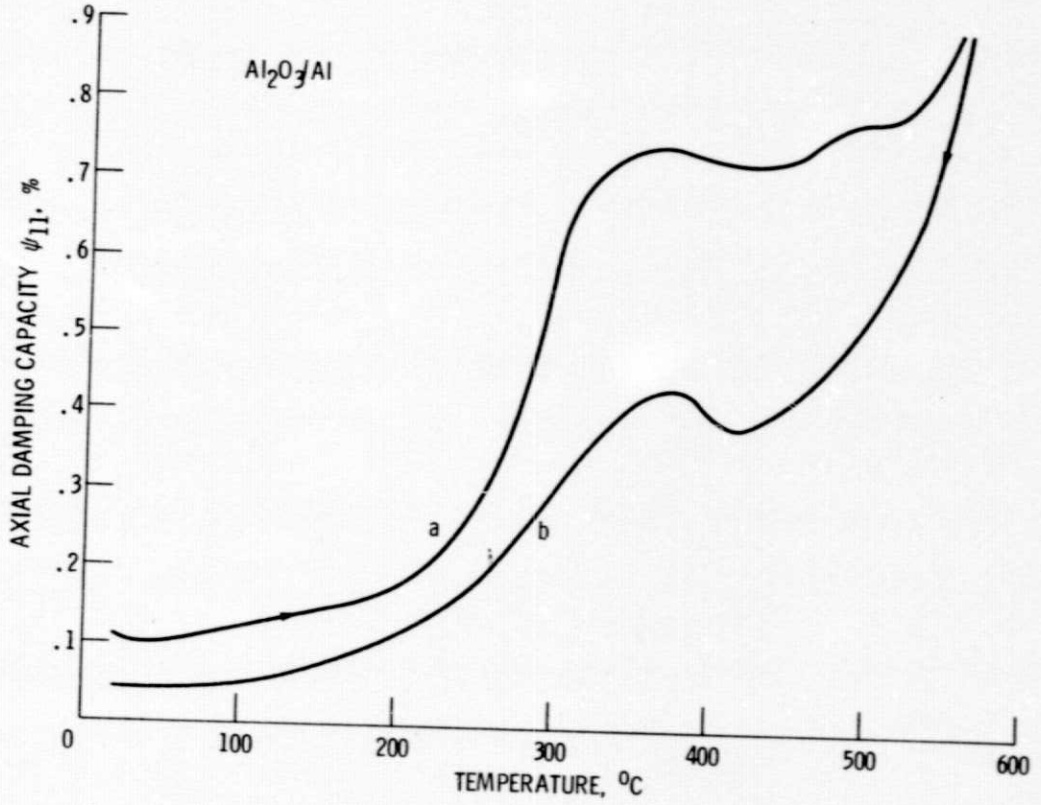

Figure 7. - Temperature dependence of damping for the Al_2O_3/Al axial specimen in the as-fabricated (curve a) and heat-treated at 560° C (curve b) conditions. Measurements were made near 2100 Hz at strains $< 10^{-6}$.

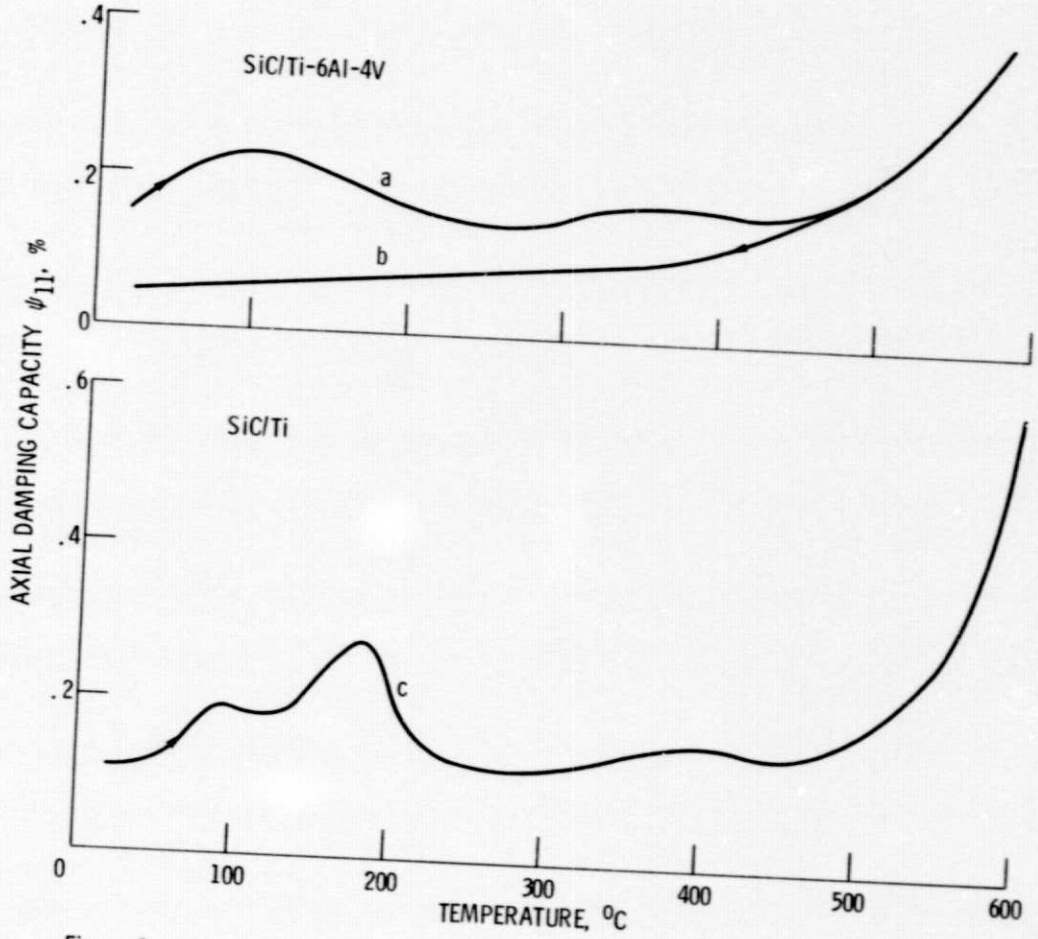

Figure 8. - Temperature dependence of damping for the SiC/Ti-6Al-4V axial specimen in the as-fabricated (curve a) and heat-treated at 590° C (curve b) conditions, and for the SiC/Ti axial specimen in the as-fabricated condition (curve c). Measurements were made near 2100 Hz and 1200 Hz, respectively, and at strains $< 10^{-6}$.

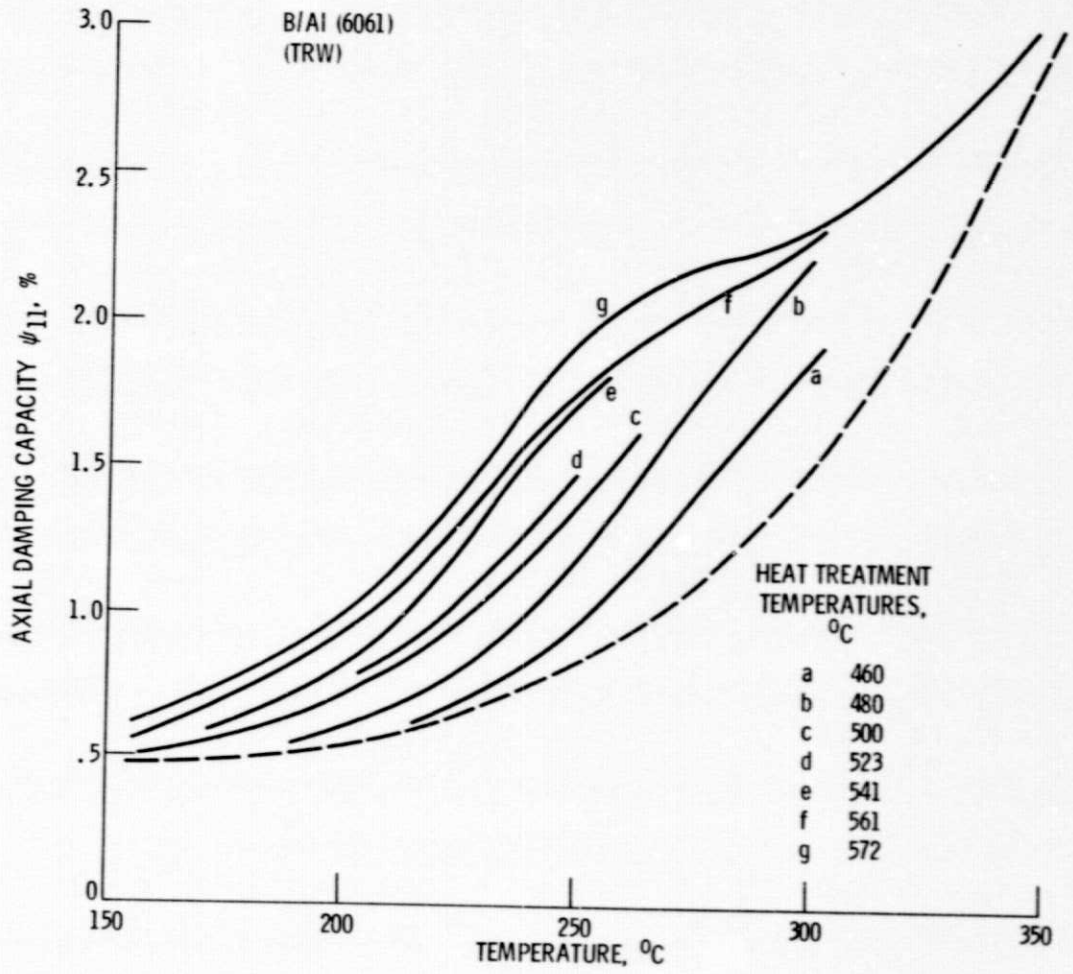

Figure 9. - Damping for a TRW B/Al (6061) axial specimen after consecutive 1-hour heat treatments at the indicated temperatures. Measurements were made near 2000 Hz at strains $< 10^{-6}$. The dashed background curve is curve a of figure 3.

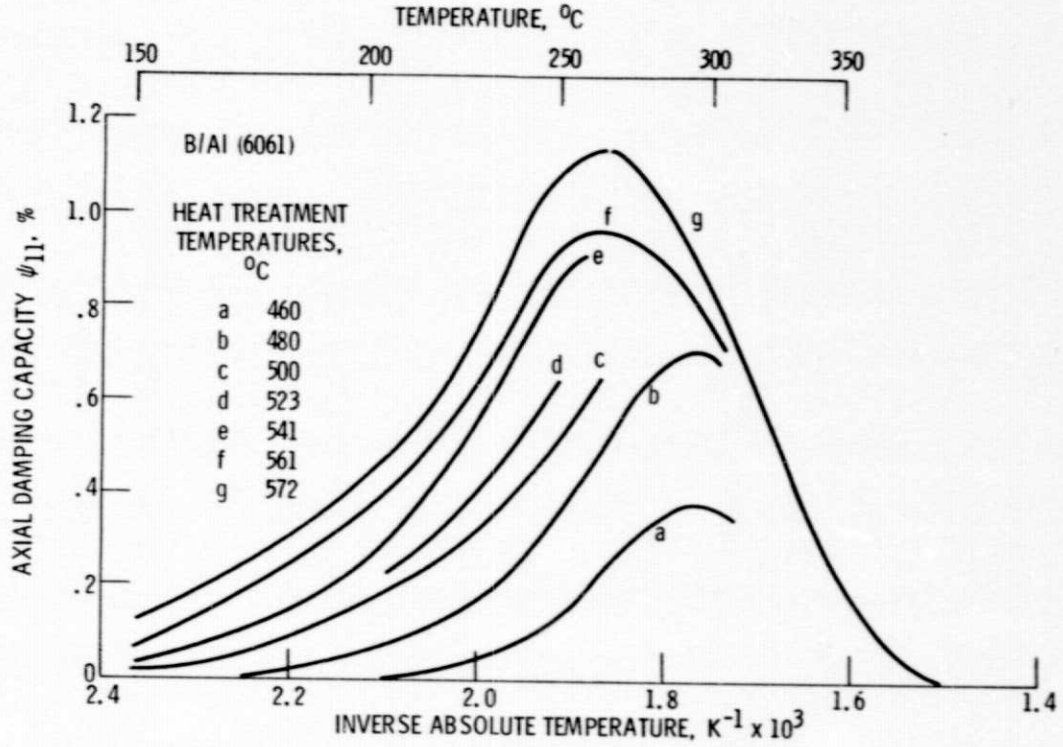

Figure 10. - Damping growth for a TRW B/Al (6061) axial specimen after consecutive 1-hour heat treatments at the indicated temperatures. Curves were determined by subtracting background damping from damping data measured near 2000 Hz at strains $< 10^{-6}$.

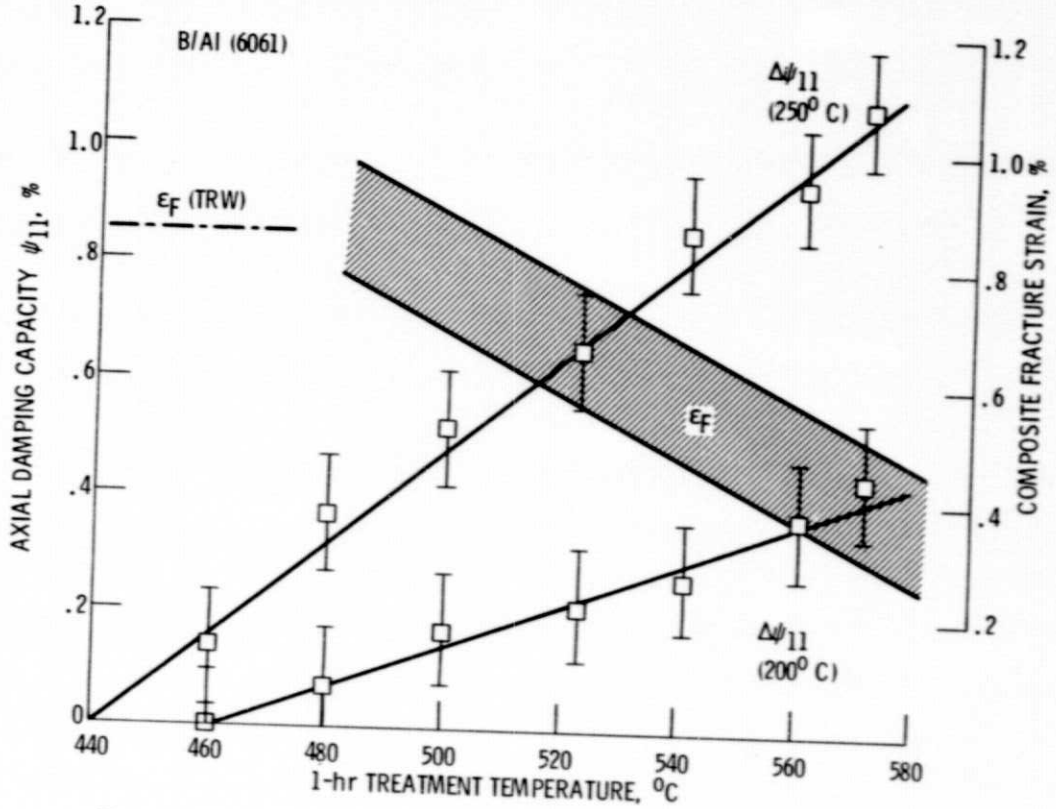

Figure 11. - Effects of 1-hour heat treatments on B/Al fracture strain (ref. 19) and on the damping growth at 200° C and 250° C for a TRW B/Al (6061) axial specimen. Damping was measured near 2000 Hz at strains $< 10^{-6}$. The dash-dot line is the estimated fracture strain for the TRW specimen in the as-fabricated condition.

ORIGINAL PAGE IS
OF POOR QUALITY